

Isotropic piezoresistance of p-type 4H-SiC in (0001) plane

Cite as: Appl. Phys. Lett. **113**, 012104 (2018); <https://doi.org/10.1063/1.5037545>

Submitted: 25 April 2018 . Accepted: 17 June 2018 . Published Online: 03 July 2018

Tuan-Khoa Nguyen , Hoang-Phuong Phan , Toan Dinh , Toshiyuki Toriyama, Koichi Nakamura, Abu Riduan Md Foisal, Nam-Trung Nguyen , and Dzung Viet Dao



View Online



Export Citation



CrossMark

ARTICLES YOU MAY BE INTERESTED IN

[Direct observation of stacking fault shrinkage in 4H-SiC at high temperatures by in-situ X-ray topography using monochromatic synchrotron radiation](#)

Applied Physics Letters **113**, 012101 (2018); <https://doi.org/10.1063/1.5038189>

[Fundamental piezoresistive coefficients of p-type single crystalline 3C-SiC](#)

Applied Physics Letters **104**, 111905 (2014); <https://doi.org/10.1063/1.4869151>

[Enhanced n-doping of epitaxial graphene on SiC by bismuth](#)

Applied Physics Letters **113**, 011602 (2018); <https://doi.org/10.1063/1.5029541>

Lock-in Amplifiers
up to 600 MHz



Watch



Isotropic piezoresistance of p-type 4H-SiC in (0001) plane

Tuan-Khoa Nguyen,^{1,a)} Hoang-Phuong Phan,¹ Toan Dinh,¹ Toshiyuki Toriyama,² Koichi Nakamura,^{3,4} Abu Riduan Md Foisal,¹ Nam-Trung Nguyen,¹ and Dzung Viet Dao^{1,5}

¹Queensland Micro- and Nanotechnology Centre, Griffith University, 170 Kessels Road, Brisbane, Queensland 4111, Australia

²Department of Mechanical Engineering, College of Science and Engineering, Ritsumeikan University, 1-1-1 Noji-higashi, Kusatsu, Shiga 525-8577, Japan

³Center for the Promotion of Interdisciplinary Education and Research, Kyoto University, Kyoto 615-8540, Japan

⁴Department of Materials Science and Engineering, Egypt-Japan University of Science and Technology, New Borg El-Arab, Alexandria 21934, Egypt

⁵School of Engineering and Built Environment, Griffith University, Parklands Drive, Gold Coast, Queensland 4215, Australia

(Received 25 April 2018; accepted 17 June 2018; published online 3 July 2018)

In this work, the isotropic piezoresistance in the (0001) plane of p-type 4H-SiC was discovered by means of the hole energy shift calculation and the coordinate transformation. These results were also confirmed by the measurement of the piezoresistance using a bending beam method. The fundamental longitudinal and transverse piezoresistive coefficients π_{11} and π_{12} were found to be $6.43 \times 10^{-11} \text{ Pa}^{-1}$ and $-5.12 \times 10^{-11} \text{ Pa}^{-1}$, respectively. The isotropy of the piezoresistance in the basal plane of p-type 4H-SiC is attributed to the isotropic hole energy shift under uniaxial strain. This interesting phenomenon in p-type 4H-SiC is promising for the design and fabrication of mechanical sensors and strain-engineered electronics since high sensitivity and consistent performance can be achieved regardless of the crystallographic orientation. *Published by AIP Publishing.*
<https://doi.org/10.1063/1.5037545>

Since the pioneering discovery by Smith,¹ the large change in resistivity upon applied stress/strain in semiconductors, namely, the piezoresistive (PZR) effect, has attracted great attention, reflecting in a vast number of studies and applications for mechanical sensing and strain engineering.²⁻⁶ Such an effect could also be magnified in nanoscale devices,⁷⁻⁹ which has been employed in highly sensitive and miniaturized Si-based devices [e.g., accelerometers, pressure sensors, and atomic force microscopy (AFM) probes]. Si remains the dominant material for the PZR effect in mechanical sensing. However, Si exhibits several limitations due to its intrinsic physical properties, such as the plastic deformation at a temperature above 500 °C and the instability of electrical conductance in high temperature operations.¹⁰ To push the sensing devices beyond their current limits, recent advances in the growth and fabrication technologies enable the development of SiC-based devices, which can inherit the current readiness of the Si technology and be utilized in harsh environmental applications. The strong covalent Si-C bond and wide energy bandgap of SiC lead to superior properties such as high mechanical strength, high shock resistance, chemical inertness, and thermal/electronic stability.^{11,12} Furthermore, its good compatibility with micro-machined fabrication processes positions SiC as a promising material for mechanical sensing in harsh environments.^{13,14}

The PZR effect and strain-induced mobility enhancement of Si have been well established.¹⁵ As such, the piezoresistance of Si was graphically presented in the works of Kanda,^{16,17} in which an anisotropic characteristic has been realized. Subsequently, numerous studies have been dedicated

to the understanding of the phenomenon in different SiC polytypes. For instance, the fundamental PZR coefficients in arbitrary crystallographic orientations of 3C-SiC have been revealed with a relatively high shear PZR coefficient.¹⁸ For hexagonal lattices, a high piezoresistance was realized in highly doped n-type and p-type 6H-SiC.¹⁹ By conducting the tensor transformation in n-type 6H-SiC, a wurtzite crystal, it was suggested that in the (0001) plane, the anisotropic part of the piezoresistance vanishes, whereas only the isotropic component remains.²⁰ The piezoresistivity of n-type 4H-SiC was theoretically investigated by the first principles simulation, indicating the significant gauge factor (GF) at either room or high temperature.²¹

In contrast to heterostructure devices, the use of bulk 4H-SiC can eliminate the thermal expansion mismatch between the sensing layer and the substrate (which are made of different materials), pushing the temperature limit of the sensing devices which can work in extreme environments. Moreover, 4H-SiC possesses a very high energy bandgap of 3.23 eV (three times higher than that of Si), which significantly minimizes the generation of thermally activated electron-hole pairs, contributing to the good reliability of 4H-SiC based devices in harsh environments. Although many efforts have been made for the investigation of the PZR effect in SiC, to date, the fundamental PZR coefficients of 4H-SiC, one of the most important SiC polytypes for mechanical sensors and high-power electronics devices, have not been elucidated in terms of either theoretical analysis or experimental verification. Understanding such a phenomenon in 4H-SiC not only optimizes the sensors' sensitivity but also enhances the devices' mobility by means of strain engineering. Therefore, this paper aims to theoretically and experimentally investigate the

^{a)}Email: khoa.nguyentuan@griffithuni.edu.au

fundamental PZR coefficients of 4H-SiC in the (0001) plane. As such, the longitudinal and transverse PZR coefficients were found to be $6.43 \times 10^{-11} \text{ Pa}^{-1}$ and $-5.12 \times 10^{-11} \text{ Pa}^{-1}$, respectively. Additionally, the theoretical analysis by calculating hole energy shift and coordinate transformation is in good agreement with the experimental result of the isotropic and large piezoresistances in the (0001) plane of p-type 4H-SiC. This finding is useful for the design and fabrication of mechanical sensors since the anisotropy and complexity of the PZR effect are eliminated.

Figure 1(a) shows a scanning electron microscopy (SEM) image of p-type 4H-SiC piezoresistors aligned in the $\langle 0\bar{1}10 \rangle$ orientation. The piezoresistors were located on numerous rectangular samples which were arranged in various orientations in a $350 \mu\text{m}$ -thick 4-in. epitaxial 4H-SiC (0001) wafer, as shown in Fig. 1(b). The wafer has a $1\text{-}\mu\text{m}$ -p-type epitaxial layer (with the hole concentration of 10^{18} cm^{-3}) lying on a 10^{18} cm^{-3} doped n-type 4H-SiC layer to form a p-n junction. The substrate was low doped 4H-SiC. The mesa p-type piezoresistors were fabricated by conventional lithography and

inductive plasma etching (ICP). It should be noted that the final etch depth of the p-type layer was $1.3 \mu\text{m}$, which ensures that the designated areas in the layer are completely etched. To form the contact, titanium and aluminum layers, with the same thickness of 100 nm , were subsequently sputtered on the wafer followed by wet etching using Al and Ti etchants. The piezoresistors have the length and width varying from $20 \mu\text{m}$ to $200 \mu\text{m}$ and $5 \mu\text{m}$ to $80 \mu\text{m}$, respectively. High temperature annealing was performed to obtain a good Ohmic contact from Ti/Al to p-type 4H-SiC, showing linear current-voltage characteristics in a voltage range from -2 V to 2 V . The detailed annealing condition was reported elsewhere in which the metal contact was annealed up to 1000°C in a nitrogen atmosphere.²² Finally, the wafer was diced into $30 \times 3 \text{ mm}^2$ beams for the bending experiment.

The current leakage through the p-n junction between p-type and n-type layers was measured and found to be four orders of magnitude smaller than the current flowing in the p-type piezoresistors. This is attributed to the robust p-n junction acting as a back-to-back diode which prevents the electric current leaking to the n-type layer.^{22,23} Therefore, it can be concluded that only the p-type layer contributed to the PZR measurement.

The straining configuration using a bending beam method to induce uniaxial strain/stress to the piezoresistors is illustrated in Fig. 2(a). The piezoresistors were designed in the vicinity of the clamping area to maximize the induced strain. Since the p-type layer is much thinner than the total thickness of the beam (i.e., $1 \mu\text{m}$ vs $350 \mu\text{m}$), the uniaxial strain would be effectively transferred to the top p-type layer.¹⁸ Let F be the applied force at the free end of the beam, and then, the induced stress can be deduced as $\sigma = 6Fl/bt^2$, where, l , b , and t are the length, width, and thickness of the 4H-SiC beam, respectively. Additionally, the uniformity of strain induced into the top p-type layer was confirmed using a finite element analysis, which is independent of the width and length of the piezoresistor (see Sec. 1 in the [supplementary material](#)). Figure 2(b) shows the measurement results of the PZR effect of p-type 4H-SiC aligned in various orientations in the (0001) plane at room temperature (i.e., 298 K). The longitudinal and transverse piezoresistors were fabricated in all beams in order to investigate the piezoresistive effect in different orientations in the plane. Subsequently, the relative resistance changes were measured against a varying induced strain from 0 to 557 ppm . The variation of the resistance in either the longitudinal or the transverse piezoresistor is proportional to the increasing strain, indicating a good linearity of the PZR effect in 4H-SiC. The consistent gauge factor (GF) in different orientations exhibits the isotropic piezoresistance of p-type 4H-SiC in the (0001) plane. The small tolerance among these results is attributed to the fact that the source wafer has the 4° off-cut surface towards the $\langle 11\bar{2}0 \rangle$ orientation from the ideal basal plane.

The PZR coefficients, typically represented in an arbitrarily oriented coordinate system, can be calculated from a tensor transformation. The resistivity tensor ρ of 4H-SiC is given in the relationship between the electric potential E and current density J in the principal coordinate (i.e., O-xyz) as $E = \rho J$, where E and J are the first rank tensors and ρ is a second rank tensor. By applying a coordinate transformation

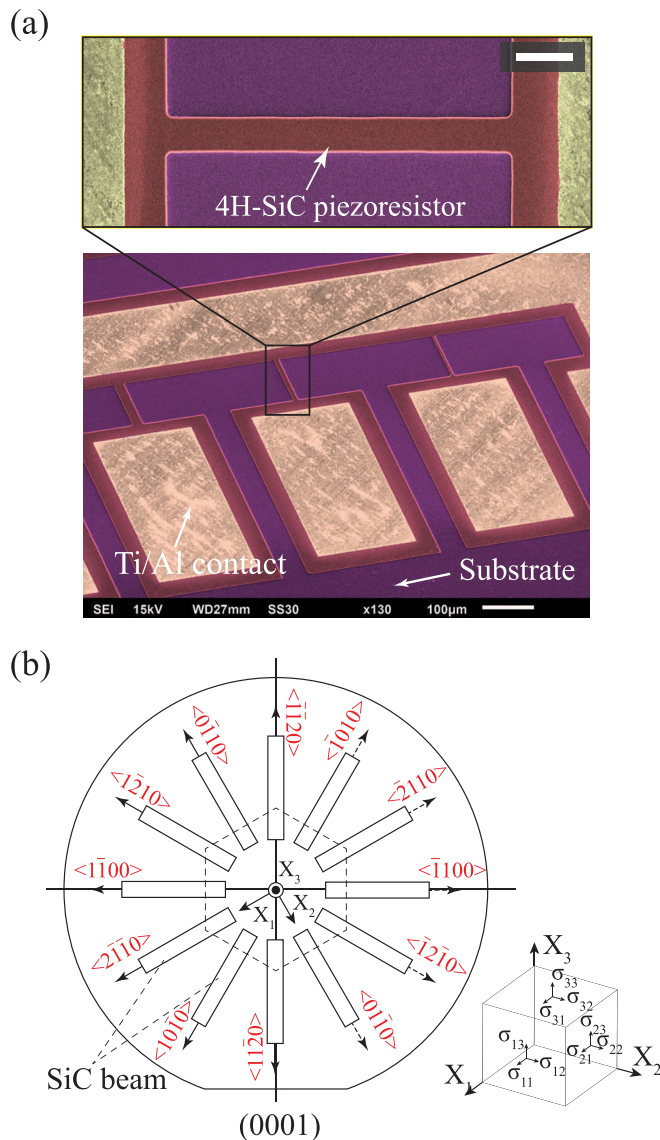


FIG. 1. (a) SEM image of 4H-SiC piezoresistors in the $\langle 0\bar{1}10 \rangle$ orientation. Top image: Scale bar, $20 \mu\text{m}$. (b) 4H-SiC beams aligned in different orientations in a full (0001) wafer. Inset: Stress tensor in the Cartesian coordinate.

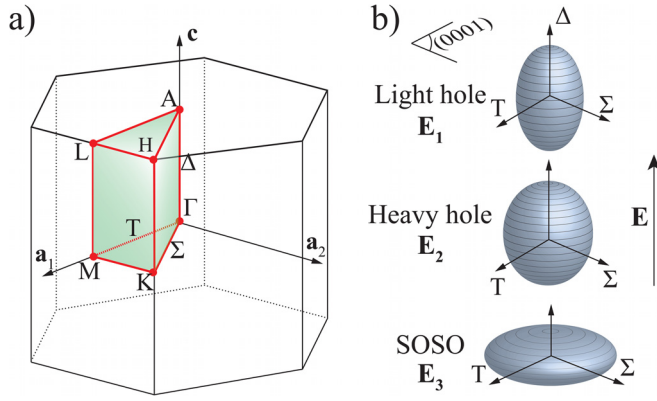


FIG. 4. (a) First Brillouin zone of 4H-SiC with high symmetry points in k -space. (b) Representation of the constant energy surfaces for the three highest valence bands in 4H-SiC.²⁴ From top to bottom: Light hole, heavy hole, and spin orbit split-off (SOSO) bands, respectively.

and simultaneously lower the heavy hole (HH) bands parallel to the stress orientation because of the change in the overlap between the atomic orbitals. Figure 4(b) shows the constant energy surfaces for three topmost valence bands without strain in 4H-SiC, showing ellipsoidal shapes.²⁴ The isotropic piezoresistance can be determined by the hole energy shift of the valence bands at $\mathbf{k} = 0$ under strain. According to Bir,²⁶ the energy of the three topmost valence bands at $\mathbf{k} = 0$ in the unstrained 4H-SiC crystal is

$$E_1^0 = \Delta_1 + \Delta_2, \quad (2)$$

$$E_{2,3}^0 = \frac{\Delta_1 - \Delta_2}{2} \pm \sqrt{\left(\frac{\Delta_1 - \Delta_2}{2}\right)^2 + 2\Delta_3^2},$$

where $\Delta_i (i = 1, 2, 3)$ are the spinor representations for the symmetry points in the Brillouin zone. The first order approximation for the strained band energy $E(\mathbf{k}, \epsilon)$ is

$$E_1^s = F, \quad (3)$$

$$E_{2,3}^s = \frac{G + \lambda}{2} \pm \sqrt{\left(\frac{G - \lambda}{2}\right)^2 + \Delta^2},$$

where $\Delta = \sqrt{2}\Delta_3$; $F = \Delta_1 + \Delta_2 + \lambda + \theta$; $G = \Delta_1 - \Delta_2 + \lambda + \theta$; $\lambda = A_1k_z^2 + A_2(k_x^2 + k_y^2) + D_1\epsilon_{zz} + D_2(\epsilon_{xx} + \epsilon_{yy})$; $\theta = A_3k_z^2 + A_4(k_x^2 + k_y^2) + D_3\epsilon_{zz} + D_4(\epsilon_{xx} + \epsilon_{yy})$; ϵ is the strain component; k_x , k_y , and k_z are the vectors in the k -space; and A_i are the components of the Hamiltonian matrix of the 4H-SiC crystal. The four deformation potential constants D_1 , D_2 , D_3 , and D_4 determine the complete band warpage due to the elastic deformation. The components $A_1k_z^2 + A_2(k_x^2 + k_y^2)$ and $A_3k_z^2 + A_4(k_x^2 + k_y^2)$ indicate that the constant energy surface is the ellipsoid of the revolution around the c -axis without strain [Fig. 4(b)]. The ratios of holes occupied in the top valence subband (E_1) versus the second highest subband E_2 (P_1/P_2) and the spin orbit split-off (SOSO) subband E_3 (P_1/P_3) are $e^{\Delta E_{1-2}/k_B T}$ and $e^{\Delta E_{1-3}/k_B T}$, respectively (see Sec. 4 in the [supplementary material](#) for the explanation). From the band structure of 4H-SiC,²⁷ we derive $\Delta E_{1-2} = 0.15$ eV and $\Delta E_{1-3} = 0.8$ eV. Substituting $k_B = 1.38 \times 10^{-23}$ m² kg s⁻² K⁻¹ and $T = 298$ K, we have $P_1/P_2 = 365$ and $P_1/P_3 = 4.83 \times 10^{13}$. This indicates that the number of holes in the highest

subband E_1 is dominant over the other two subbands E_2 and E_3 . Therefore, the piezoresistance of 4H-SiC is solely dictated by the hole redistribution in E_1 under strain (see Sec. 4 in the [supplementary material](#)). The hole energy shift in E_1 under strain was then obtained by $\Delta E_1 = E_1^s - E_1^0 = \lambda + \theta$.

Due to the hexagonal symmetry in the compliance tensor of 4H-SiC, a uniaxial stress σ_{xx} is equivalent to biaxial strains in the hexagonal basal plane as

$$\epsilon_{xx} + \epsilon_{yy} = (S_{11} + S_{21})\sigma_{xx}; \quad \epsilon_{zz} = S_{31}\sigma_{xx}, \quad (4)$$

where S_{ij} are the components of the compliance tensor of 4H-SiC. Three components of the strain tensor ϵ_{xx} , ϵ_{yy} , and ϵ_{zz} are isotropic under coordinate transformation around the c -axis which is perpendicular to the basal plane, i.e., the transversely isotropic property of Hooke's law applied for the hexagonal lattice. Thus, $\lambda = A_1k_z^2 + A_2(k_x^2 + k_y^2) + D_1S_{31}\sigma_{xx} + D_2(S_{11} + S_{21})\sigma_{xx}$ and $\theta = A_3k_z^2 + A_4(k_x^2 + k_y^2) + D_3S_{31}\sigma_{xx} + D_4(S_{11} + S_{21})\sigma_{xx}$ are also isotropic under the coordinate transformation around the c -axis. Conducting the second derivative of E_1 with respect to k_x , k_y , and k_z in k -space, we have $\partial^2 E_1^s / \partial k_j^2 \equiv \partial^2 E_1^0 / \partial k_j^2$, where $j = (x, y, z)$ (see Sec. 5 in the [supplementary material](#)). This indicates that the variation of the energy in the subband E_1 is independent of the strain direction in the (0001) plane, exhibiting the isotropic hole energy shift ΔE_1 under a uniaxial stress σ_{xx} on the basal plane.

In contrast to the anisotropy of the PZR effect in several common semiconductors (e.g., Si and 3C-SiC), the piezoresistance in 4H-SiC exhibits an isotropic property, which is more favorable for the design and fabrication of mechanical sensors, as the need for choosing the optimal orientation is no longer needed. As a result, high sensitivity can be achieved regardless of the arrangement of devices in wafers, and the number of devices per wafer can be significantly increased, reducing the cost for the sensing device.

In conclusion, the isotropic piezoresistance in the (0001) plane of p-type 4H-SiC was discovered by the calculations of the hole energy shift in the top valence bands and the coordinate transformation. The interesting phenomenon was also verified by the experimental results using a bending beam method where a uniaxial strain was applied to the piezoresistor. The longitudinal and transverse PZR coefficients were found to be 6.43×10^{-11} Pa⁻¹ and -5.12×10^{-11} Pa⁻¹, respectively, which are independent of the strain orientation in the (0001) plane. The isotropic piezoresistance of p-type 4H-SiC is attributed to the isotropic hole energy shift under uniaxial stress/strain in the basal plane. For calculating the parameters for each subband in bulk p-type 4H-SiC, more effort is required, and the data will be presented in our future work. The relatively high and isotropic piezoresistivity of p-type 4H-SiC is promising for mechanical sensing and strain engineering since a high sensitivity can be achieved regardless of the sensor orientation.

See [supplementary material](#) for the details of the strain distribution in the bending beam configuration, the measured Young's modulus in various orientations in the (0001) plane, the matrix transformation from the principal coordinate to an arbitrary coordinate, the calculation of the hole occupation in

the valence subbands, and the valence subband modification under strain.

This work was partially supported by Australian Research Council Grant Nos. LP150100153 and LP160101553. This work was also supported by the Queensland node of the Australian National Fabrication Facility, a company established under the National Collaborative Research Infrastructure Strategy to provide nano- and micro-fabrication facilities for Australian researchers.

- ¹C. S. Smith, *Phys. Rev.* **94**, 42 (1954).
- ²P. Kleimann, B. Semmache, M. L. Berre, and D. Barbier, *Phys. Rev. B* **57**, 8966 (1998).
- ³T.-K. Nguyen, H.-P. Phan, J. Han, T. Dinh, A. R. M. Faisal, S. Dimitrijević, Y. Zhu, N.-T. Nguyen, and D. V. Dao, *RSC Adv.* **8**, 3009 (2018).
- ⁴N. Minh-Dung, H.-P. Phan, K. Matsumoto, and L. Shimoyama, *IEEE MEMS* 617 (2013).
- ⁵H. Peelaers and C. G. V. de Walle, *Phys. Rev. B* **86**, 241401(R) (2012).
- ⁶H.-P. Phan, T. Dinh, T. Kozeki, T.-K. Nguyen, A. Qamar, T. Namazu, N.-T. Nguyen, and D. V. Dao, *IEEE Electron Device Lett.* **37**, 1029 (2016).
- ⁷J. S. Milne, A. C. H. Rowe, S. Arscott, and C. Renner, *Phys. Rev. Lett.* **105**, 226802 (2010).
- ⁸J. Bi, G. Wei, L. Wang, F. Gao, J. Zheng, B. Tang, and W. Yang, *J. Mater. Chem. C* **1**, 4514 (2013).
- ⁹F. Gao, J. Zheng, M. Wang, G. Wei, and W. Yang, *Chem. Commun.* **47**, 11993 (2011).
- ¹⁰I. Yonenaga, *J. Mater. Sci.: Mater. Electron.* **14**, 279 (2003).
- ¹¹T.-K. Nguyen, H.-P. Phan, H. Kamble, R. Vadivelu, T. Dinh, A. Iacopi, G. Walker, L. Hold, N.-T. Nguyen, and D. V. Dao, *ACS Appl. Mater. Interfaces* **9**, 41641 (2017).
- ¹²H.-P. Phan, T.-K. Nguyen, T. Dinh, G. Ina, A. R. Kermany, A. Qamar, J. Han, T. Namazu, R. Maeda, D. V. Dao, and N.-T. Nguyen, *Appl. Phys. Lett.* **110**, 141906 (2017).
- ¹³H.-P. Phan, T. Dinh, T. Kozeki, T.-K. Nguyen, A. Qamar, T. Namazu, N.-T. Nguyen, and D. V. Dao, *Appl. Phys. Lett.* **109**, 123502 (2016).
- ¹⁴D. Senesky, B. Jamshidi, K. B. Cheng, and A. Pisano, *IEEE Sens. J.* **9**, 1472 (2009).
- ¹⁵M. Chu, Y. Sun, U. Aghoram, and S. E. Thompson, *Annu. Rev. Mater. Res.* **39**, 203 (2009).
- ¹⁶Y. Kanda, *IEEE Trans. Electron Devices* **29**, 64 (1982).
- ¹⁷Y. Kanda and K. Suzuki, *Phys. Rev. B* **43**, 6754 (1991).
- ¹⁸H.-P. Phan, D. V. Dao, P. Tanner, L. Wang, N.-T. Nguyen, Y. Zhu, and S. Dimitrijević, *Appl. Phys. Lett.* **104**, 111905 (2014).
- ¹⁹R. Okojie, A. Ned, A. Kurtz, and W. Carr, *IEEE Trans. Electron Devices* **45**, 785 (1998).
- ²⁰T. Toriyama, *J. Micromech. Microeng.* **14**, 1445 (2004).
- ²¹K. Nakamura, T. Toriyama, and S. Sugiyama, *Jpn. J. Appl. Phys.* **50**, 06GE05 (2011).
- ²²T.-K. Nguyen, H.-P. Phan, T. Dinh, J. Han, S. Dimitrijević, P. Tanner, A. R. M. Faisal, Y. Zhu, N.-T. Nguyen, and D. V. Dao, *IEEE Electron Device Lett.* **38**, 955 (2017).
- ²³T. Akiyama, D. Briand, and N. F. de Rooij, *J. Micromech. Microeng.* **22**, 085034 (2012).
- ²⁴C. Persson and U. Lindefelt, *Phys. Rev. B* **54**, 10257 (1996).
- ²⁵J. S. Milne, I. Favorskiy, A. C. H. Rowe, S. Arscott, and C. Renner, *Phys. Rev. Lett.* **108**, 256801 (2012).
- ²⁶G. L. Bir, *Symmetry and Strain-Induced Effects in Semiconductors* (Wiley, 1974).
- ²⁷C. Persson and U. Lindefelt, *J. Appl. Phys.* **82**, 5496 (1997).